Supporting Online Material for

The Ribosome Modulates Nascent Protein Folding

Christian M. Kaiser, Daniel H. Goldman, John D. Chodera, Ignacio Tinoco Jr., Carlos Bustamante*

*To whom correspondence should be addressed. E-mail: carlos@alice.berkeley.edu

Published 23 December 2011, *Science* **334**, 1723 (2011)
DOI: 10.1126/science.1209740

This PDF file includes:

Materials and Methods

Preparation of derivatized ribosomes

To generate a unique attachment site within the 50S ribosomal subunit, we targeted the C-terminus of the large ribosomal subunit protein L17. L17 was selected for its location away from the ribosomal subunit interface and from the immediate vicinity of the ribosomal exit tunnel. We chromosomally replaced the open reading frame of *rplQ*, the single gene encoding L17 in *Escherichia coli*, with the coding sequence of C-terminally ybbR tagged (*50*) L17 in *E. coli* strain MC4100 using the phage λ Red recombinase system as described (*51*). The plasmids and strains for the Red recombinase system were generously provided by Prof. Barry Wanner (Purdue University). A tetracyclin resistance gene was used as the selection marker. The resulting strain produces ribosomal protein L17 with a C-terminal ybbR-tag. Engineered ribosomes were isolated from the recombinant strain as described previously (*52*) and stored frozen.

The serine residue at position 2 in the 11 amino acid (aa) long ybbR tag sequence (*50*) serves as an acceptor of the phosphopantethein moiety of Coenzyme A (CoA) in an enzymatic reaction catalyzed by the phosphopantethein transferase Sfp from *Bacillus subtilis* (*50*). It has been shown that the thiol group of CoA can be derivatized with chemical moieties such as fluorophores without interfering with the specificity or efficiency of the Sfp-mediated reaction (*50*). The expression plasmid for the Sfp enzyme was generously provided by Prof. Christopher Walsh (Harvard Medical School). The protein was expressed and purified as described (*53*).

To demonstrate the specificity of the reaction in the chemically complex environment of the ribosome, we derivatized purified engineered ribosomes with a fluorescent CoA-adduct (F-CoA) prepared by reacting reduced CoA (Fisher Scientific) with fluorescein-5-maleimide (Invitrogen). The covalent attachment of the fluorescent phosphopantethein-fluorescein moiety allows in-gel detection of the labeled L17 protein after separation by SDS-PAGE (Supplementary Figure S1). As expected, a single fluorescent band was detected after incubating engineered ribosomes (5 μM) with F-CoA (10 μM) and purified Sfp enzyme (1.5 μM). Labeling was dependent on the presence of the ybbR tag sequence on L17, the CoA moiety and the Sfp enzyme, confirming the specificity of the reaction in this system.

To covalently couple a DNA handle to L17, we repeated the reaction replacing F-CoA with a 25 nucleotide (nt) long oligonucleotide that was chemically modified at its 5'-end with CoA and hybridized to a shorter, complementary oligonucleotide prior to the reaction, resulting in a double-stranded (ds) oligonucleotide with a 4 nt long single stranded overhang. Unreacted oligonucleotide was removed by sedimenting the derivatized ribosomes through a 1M sucrose cushion. To assess the efficiency of the reaction, an aliquot of the derivatized ribosomes was subsequently reacted with F-CoA. From quantitation of the in-gel fluorescence and the amount of ribosomes, we estimated that derivatization with the DNA handle was ≥ 50% efficient.

Generation of ribosome-nascent chain complexes (RNCs)

We used messenger RNAs (mRNAs) lacking stop codons as templates for *in vitro* translation reactions. If the ribosome does not encounter an in-frame stop codon, termination of translation and nascent chain release do not occur. The ribosome proceeds to the 3'-end of the mRNA and stalls there. As a consequence, the translation product

accumulates as a ribosome-bound peptidyl-tRNA species. Thus, we can precisely determine where the ribosome stalls by choosing the appropriate mRNA template. To produce specific templates, we first amplified specific regions of the T4 lysozyme construct shown in Figure 1D using the polymerase chain reaction (PCR) with specific primers. PCR products were gel-purified and served as templates in *in vitro* transcription reactions yielding mRNA (T7 MegaScript Kit, Ambion). The mRNA was isolated (MegaClear Kit, Ambion) and used as a template in *in vitro* translation reactions.

We generated T4 lysozyme constructs that harbored an N-terminal Avi tag sequence by subcloning. The T4 lysozyme source plasmid was a gift from Prof. Susan Marqusee (University of California, Berkeley). The Avi tag is recognized by the *E. coli* biotin ligase BirA with high specificity (*54*). BirA covalently modifies Lys10 in the 15 residue Avi tag sequence with a biotin moiety. The extraordinarily strong biotin-streptavidin interaction has previously been utilized to immobilize macromolecules for optical tweezers experiments (*55*) and provides an attachment point near the N-terminus of the T4 lysozyme constructs in our experiments. We cloned the *birA* gene into an expression vector and purified the protein by means of an engineered His_6 tag.

Translation reactions were carried out using the PURE *in vitro* protein synthesis system (*56*). We utilized a ribosome-free version of this Kit (PURExpress Δ Ribosome Kit, New England Biolabs) supplemented with engineered ribosomes (~1 μM) and purified mRNA template (~5 μM). We chose to use a molar excess of template over ribosomes to minimize the initiation of more than one ribosome per template molecule which would result in polysome formation and product heterogeneity. *In vitro* translation reactions also contained 50 μM D-biotin and 0.5 – 1 μM purified BirA enzyme. Translation was carried out for 30 min at 37°C. Reactions were chilled on ice and briefly clarified by centrifugation (10 min, 16,000 *g*, 4°C). Ribosome-nascent chain complexes were sedimented through a 1M sucrose cushion in Buffer HKM (25 mM HEPES-KOH pH 7.4, 150 mM KCl, 5 mM Mg-acetate) by centrifugation for 40 min at 200,000 *g*, 4°C. The supernatant was discarded and the pelleted ribosome-nascent chain complexes were resuspended in a small volume of Buffer HKM.

Translation products were analyzed in bulk by SDS-PAGE followed by detection with Streptavidin-HRP (Southern Biotech) after electro-blotting onto a nitrocellulose membrane. As expected, the ribosome-bound nascent polypeptides accumulated as an RNase A-sensitive peptidyl-tRNA species with an apparent molecular weight ~15 – 20 kDa larger than expected for the free protein (Supplementary Figure S2A). Treatment of RNCs with puromycin also led to peptidyl-tRNA hydrolysis (Supplementary Figure S2A). Since the ribosomal peptidyl-transferase activity is required for puromycin to replace the tRNA, this finding confirms that the C-terminus of the nascent polypeptide is stably anchored in the peptidyl-transferase center, as predicted based on our experimental design.

Immobilization of RNCs for optical tweezers experiments

To immobilize ribosome-nascent chain complexes on the surface of a polystyrene microsphere for manipulation with optical tweezers, we functionalized the surface of 2.1 μm carboxyl-polystyrene beads (Spherotech) with double-stranded DNA oligonucleotides. The double-stranded oligonucleotides contained an amino-modifier on one of the 5'-ends and a 4 nt single-stranded overhang on the other. The DNA was covalently coupled to the bead surface by chemical crosslinking with 1-ethyl-3-[3-

dimethylaminopropyl] carbodiimide hydrochloride (EDC; Pierce Protein Research Products) as described (*57*). The reaction was quenched with 50 mM Tris-HCl, pH 7.6, and the beads were washed extensively to remove free oligonucleotides.

The single-stranded overhang at the distal end of the oligonucleotide was designed to be complementary to that of the oligonucleotide attached to ribosomal protein L17 (see above). It thus provides a "sticky end" and allows a directed, covalent coupling of the RNCs and the functionalized beads *via* DNA ligation. After ligation, the RNCs are separated from the bead surface by 51 bp of double-stranded DNA. For ligation, beads were equilibrated in T4 DNA ligase Buffer (New England Biolabs), mixed with RNC and T4 DNA ligase (New England Biolabs), and incubated at 16°C for 30 min. The resulting "sample beads" were stored on ice until they were injected into the microchamber of the optical tweezers instrument.

Immobilization of free T4 lysozyme for optical tweezers experiments

The enzymatic reactions described above for RNCs were also used to immobilize free T4 lysozyme polypeptides on polystyrene beads. The T4 lysozyme open reading frame was subcloned into an expression vector such that it is flanked by sequences encoding an N-terminal Avi-tag and a C-terminal ybbR tag. After expression in *E. coli* and biotinylation *in vitro*, the protein was purified by affinity chromatography on monomeric avidin agarose (Pierce Protein Research Products) and size exclusion chromatography. A DNA handle was covalently linked to the C-terminal ybbR tag in an Sfp-mediated reaction as described above. To remove unreacted handle, the protein was again subjected to chromatography on monomeric avidin agarose. The derivatized protein was ligated to functionalized polystyrene beads as described above. The sample was stored on ice until injection into the microchamber of the optical tweezers instrument.

Puromycin-mediated handle attachment

We utilized oligonucleotides with a puromycin (Pm)-moiety at the 3' terminus ("Pm-oligonucleotides") to release nascent chains from stalled RNCs and simultaneously conjugate a DNA handle to the C-terminus of the released nascent chain (Supplementary Figure S2B). The ability of Pm-oligonucleotides to function as Pm analogs in nascent chain release has been demonstrated previously with RNA conjugates (*39*) and results in covalent attachment of the oligonucleotide to the C-terminal amino acid of the nascent polypeptide. We incubated purified RNCs with Pm-oligonucleotides that had previously been hybridized to yield a dsDNA oligonucleotide with a "sticky end" (see above). The resulting product was analyzed by SDS-PAGE, electro-blotting and detection with Streptavidin-HRP (Supplementary Figure S2). The released product (which we term "peptidyl-DNA") is RNase A-resistant and has an electrophoretic mobility between the free polypeptide and the peptidyl-tRNA. We ligated this product to functionalized polystyrene beads as described above.

Synthesis of immobilized DNA handles

In optical tweezers experiments, we grabbed the N-terminal end of nascent chains or the free polypeptides through a ~2kbp double-stranded DNA handle. We developed an approach to synthesize this handle directly on the polystyrene bead in a PCR-like

reaction. Carboxyl-polystyrene beads (2.1 μm diameter) were functionalized by crosslinking a single-stranded DNA oligonucleotide to the bead surface with EDC as described above. This cross-linked oligonucleotide functioned as an immobilized primer in a subsequent PCR-like reaction containing, in addition, Taq DNA polymerase (New England Biolabs), dNTPs, a linear template and a biotinylated reverse primer. The template was comprised of 1789 bp of double-stranded DNA. The ends of the template were complementary in sequence to the bead-immobilized and the free, biotinylated primer, respectively. We subjected the reactions to 35 cycles of denaturation (45 s at 94°C), annealing (45 s at 45°C) and extension (2 min at 72°C). During the reaction, the immobilized primer anneals to the template and is extended by the DNA polymerase, which also synthesizes the complementary strand after annealing of the biotinylated primer. The product is thus a double-stranded DNA fragment of 1789 bp in length. One of the 5'-ends is covalently linked to the bead surface, the other harbors a biotin moiety. Subsequently, these "handle beads" were washed extensively with TE buffer (10 mM Tris-HCl, pH 8.0, 1 mM EDTA) and stored at 4°C.

We verified successful DNA synthesis on the bead surface by injecting an aliquot of these beads into a microchamber and captured a single bead in the optical trap (see below). We readily obtained very stable tethers to a 2.1 μm streptavidin bead (Spherotech) held in a micropipette. When we stretched these tethers, we obtained the force-extension curves (Supplementary Figure S3) expected for a ~2kbp dsDNA molecule, with an overstretching plateau at ~65 pN (*55*). For experiments involving RNCs or the free protein, the biotin moiety of the bead-coupled DNA handle was derivatized with streptavidin. To this end, an aliquot of the "handle beads" was incubated with streptavidin (~2 mg/ml) for 10 min at room temperature. Subsequently, the beads were diluted 1000-fold and injected into the microchamber.

Optical tweezers measurements

We conducted our force-spectroscopy measurements on an instrument with a counterpropagating dual laser beam single trap design that measures force directly *via* the change in light momentum (*58*). Experiments were carried out in Buffer HKM using a microchamber with a micropipette. The "handle bead" is held in the optical trap, while the "sample bead" is held on the tip of the micropipette by suction. We obtained tethers by moving the optical trap relative to the chamber, bringing the beads into close proximity. To exert force, we moved the trap in the opposite direction. Force and trap-position were recorded at a sampling frequencies of 1000 Hz (force ramp measurements) or 3125 Hz (force clamp measurements). Rupture forces and extension changes from force extension curves (from force ramp measurements) were determined as described (*59*). Constant force experiments, in which the force feedback of the instrument operates at 2000 Hz, were analyzed using a Bayesian Hidden Markov Model (BHMM) approach (see below).

Several findings confirm that the rupture events observed in these measurements represent unfolding events within the nascent polypeptide: No transitions (other than overstretching of DNA at high force) are observed when the DNA handle alone is stretched (see Supplementary Figure S3). The unfolding events observed for the ribosome-bound full-length T4 lysozyme are similar to those of the free protein (see Figure 1E – H). Ribosome-bound T4 lysozyme fragments that do not acquire stable structures do not exhibit rupture events (Figure 4A). Thus, the unfolding events observed

originate from the nascent polypeptide, not from structural transitions within the ribosome.

Tethers containing ribosome-nascent chain complexes are stable up to ~50 pN of force without exhibiting unfolding transitions other than those resulting from nascent chain unfolding. At forces above 50 pN, the tether is lost due to breakage, presumably due to extraction of protein L17 (the attachment point in our geometry) from the large ribosomal subunit. Extraction of the nascent chain through the exit tunnel might also be possible, but would require unfolding of the P-site tRNA-moiety to which the stalled nascent chain remains attached in our samples.

Bayesian Hidden Markov Model (BHMM) analysis

We used a Bayesian hidden Markov model (BHMM) approach (*60*) to analyze the optical tweezers data collected in constant force mode. Hidden Markov models (HMM) have been used previously to analyze single molecule trajectories (*61*). The Bayesian extension of the standard approach of HMM analysis allows the experimental uncertainties to be directly quantified by sampling from the posterior of the model parameters (transition probabilities and Gaussian state observable distributions) given the data, rather than simply identifying the maximum-likelihood model parameters as in the traditional HMM approach. To do this, we augment the standard HMM likelihood function with a prior that enforces the physical detailed balance constraint in the transition matrix. Sampling from the posterior proceeds by a Gibbs sampling approach, alternating updates of the reversible transition matrix (*62*), the hidden state sequence, and the Gaussian state observable distributions using standard techniques.

The BHMM code we used here sampled models over the measurement histories of trap position at constant force feedback, producing estimates of average extension characterizing each state and the transition probabilities among the states, as well as confidence intervals that characterize the uncertainty in these values due to finite-sample statistics. After sub-sampling the extension data to 100 Hz to produce Markovian statistics, the method samples models consistent with the data using a Gibbs sampling strategy that assumes the extension measurements from each state (including measurement error) are normally distributed about the average extension for that state. Here, the number of states was fixed to three after verifying the three-state nature of the data by inspection of the recorded traces. The first 50 BHMM samples after starting from the maximum likelihood estimate were discarded, and 1000 samples were subsequently generated to collect statistics on average extensions and transition probabilities, as well as generate the 95% confidence intervals reported here. Matrices of rate constants K were computed from transition matrices $T(\tau)$ using the standard relationship $T(\tau) = e^{K\tau}$ through use of the matrix logarithm.

The complete implementation and validation details of this code will be described elsewhere. The manuscript is freely available *via* the arXiv.org preprint server (accession number 1108.1430). The Matlab code used for the BHMM approach can be freely obtained at

http://simtk.org/home/bhmm/

Calculations of Debye lengths at 150 mM vs 500 mM KCl

The Debye length κ^{-1} is a measure of how the electrostatic potential around a charge decays due to charge screening in a given medium. The potential around a charge drops to 1/e over a length of κ^{-1}. κ^{-1} in our aqueous buffer was estimated according to

$$\kappa^2 = \frac{e^2}{\varepsilon\varepsilon_0 k_B T}\sum_i n_i z_i^2$$

with $e = 1.6\cdot10^{-19}$ C (elementary charge), $\varepsilon = 78.5$ (relative dielectric constant for water at 25 °C), $\varepsilon_0 = 8.854\cdot10^{-12}$ $CV^{-1}m^{-1}$ (permittivity of vacuum), $k_B = 1.38\cdot10^{-23}$ JK^{-1} (Boltzmann constant), and T = 298 K. n_i is the ion concentration in ions per m^3 and z_i the ion valence for component i. For our standard buffer (Buffer HKM; 25 mM HEPES-KOH, pH 7.4, 150 mM KCl, 5 mM Mg-acetate), we obtain a Debye length of $\kappa^{-1} = 0.72$ nm (assuming that half of the HEPES molecules are deprotonated at this pH). Increasing the KCl concentration to 500 mM yields $\kappa^{-1} = 0.42$ nm, a Debye length 42% shorter than the one at 150 mM KCl.

Estimation of extension fluctuations

The time resolution in our optical tweezers measurements is fundamentally limited by the relaxation time of the polystyrene beads. The thermal fluctuations of the single molecule tether that are faster than this response time (determined by the corner frequency of the bead) are thus not resolved in our measurements.

We estimated the mean square fluctuations in the extension of the N-terminus of the unfolded protein in our single-molecule experiments using the equipartition theorem:

$$\langle x^2 \rangle = \frac{k_B T}{k}$$

with $k_B = 1.38\cdot10^{-23}$ pN nm (Boltzmann constant), and T = 298 K. k is the combined stiffness of the unfolded protein and the DNA handles. To estimate an upper bound for the stiffness, we treat the unfolded protein (164 aa) and the 1789 bp DNA handle as springs on either side of the N-terminal residue. In this case, the combined stiffness is the sum of the individual stiffnesses. We do not include any other components, such as the ribosome, in these estimations. The bead relaxes much more slowly than the DNA/protein tether (we determined a corner frequency of ~1200 Hz for the 2.1 μm diameter beads used in our experiments). We can distinguish two extreme cases: Very fast fluctuations on the timescale of μs and slower fluctuations on the timescale of ms. The fluctuations of the bead will contribute only to the slower fluctuations.

In the case of very fast fluctuations, we neglect contributions of the bead. We calculated the stiffnesses of the individual components (dsDNA handles and the unfolded polypeptide) at F = 3.6 pN, assuming a WLC model with $P_{DNA} = 53$ nm, $P_{protein} = 0.65$ nm, and contour length increments of L_C(DNA) = 0.34 nm/bp and L_C(protein) = 0.36 nm/aa. The DNA handle in our assembly is 1789 bp long, yielding $k_{dsDNA,1789bp} = 0.158$ pN/nm. The stiffness of the protein is $k_{polypeptide,\ 164aa} = 0.268$ pN/nm. Thus, the combined stiffness at 3.6 pN is k = 0.426 pN/nm, and the tether fluctuates with a root mean square (RMS) deviation of $\sqrt{\langle x^2 \rangle} = 3.1$ nm. To account for the contributions of the bead that is held in the optical trap in our geometry, we combined the trap stiffness with the DNA handle stiffness as springs connected in series:

$$\frac{1}{k_{DNA+trap}} = \frac{1}{k_{dsDNA,1789bp}} + \frac{1}{k_{trap}}$$

The stiffness of our optical trap is k_{trap} = 0.1 pN/nm. We obtain $k_{DNA+trap}$ = 0.061 pN/nm, and, combined with the unchanged polypeptide stiffness, $\sqrt{\langle x^2 \rangle}$ = 3.5 nm.

These estimates indicate that the polypeptide spends a significant fraction of the time in closer proximity to the ribosome than indicated by the measured extensions, even if held at a force of 3.6 pN. Thus, even at a Debye length of less than 1 nm, charged residues within the polypeptide chain can come close enough to the ribosome to be subject to the electrostatic potential surrounding its surface. We only account for the DNA handle and the polypeptide in the above stiffness calculations. Therefore, the values obtained for the stiffness represent upper bounds, since any additional components, such as the ribosome and the linkages will have a finite stiffness that can only lower the total stiffness of the tether. As a consequence, the fluctuations calculated from this stiffness represent a lower bound and are likely to be higher than estimated here. We assume, however, that the contributions of the ribosome to the overall stiffness are negligible in the refolding force regime, because we expect this highly ordered, folded structure to be significantly less flexible under these conditions than the unfolded polypeptide and the DNA handle.

Dimensions and stability of the T4 lysozyme folding intermediate

We observed a T4 lysozyme folding intermediate immediately prior to folding to the native state in most recordings when the C-terminal segment is allowed to exit from the ribosomal tunnel. The intermediate appears to be obligatory: Consistent with the expected exponential distribution of state lifetimes, progression through the intermediate happens too quickly to be observed at the sampling resolution in a small fraction of traces. Consequently, the transition through the intermediate during folding to the native state is observed in most, but not all of the recorded traces. We estimated the dimensions of the intermediate by analyzing extension traces recorded in force clamp mode (see Figure 2A). We limited this analysis to data obtained with the free protein, because the ribosome affects the extension of the nascent polypeptide (see Figure 3), complicating the analysis. Choosing the relatively rigid native state (*38*) as a point of reference, we find that the end-to-end extension of *I* is 10.1 nm longer than that of *N* at 5 pN (see Figure 2A), which corresponds to a difference in contour length, ΔL_C(I-N), of 26.4 nm, compared to a difference between *U* and *N*, ΔL_C(U-N), of 60.1 nm, according to the WLC model (see above). Thus, the unfolded molecule compacts by ΔL_C(U-I) = 33.7 nm upon forming the intermediate. Assuming an end-to-end distance of the intermediate in the range from 0.9 nm (the folded state end-to-end distance) to 5.0 nm (the longest Cα-distance in the folded protein), between 96 to 108 aa participate in the intermediate formation.

We used our force-clamp data to estimate the stability of the intermediate. The unfolded and intermediate states (*U* and *I*, respectively) are equally populated at a force of $F_{1/2} \approx 3.6$ pN (see Figure 2E and Suppl. Figure S8), with an extension change of $\Delta x_{U\text{-}I} \approx 10$ nm separating *U* and *I*. According to the WLC model, a change in extension of 10 nm at 3.6 pN corresponds to a change in contour length of $\Delta L_C \approx 30$ nm (assuming a persistence length for unfolded polypeptides of P = 0.65 nm). We calculated a force extension curve with these parameters (ΔL_C = 30 nm, P = 0.65 nm) and determined

ΔG(stretch) by integrating the WLC equation with boundaries F = 0 pN to F = $F_{1/2}$ = 3.6 pN. It yields ΔG(stretch)=15 pN nm. Thus, ΔG_0 = (36 - 15) pN nm = 21 pN nm = 12.7 kJ/mol = 3 kcal/mol.

A native-like "hidden" intermediate, composed largely of the C-terminal T4 lysozyme subdomain, including the N-terminal 12 aa that comprise the "A-helix" (*37, 63*), has previously been observed. The thermodynamic stability of this hidden intermediate is 7.9 kcal/mol (*29*), significantly more stable than the intermediate we observe (3.0 kcal/mol at zero force). Presumably, the N-terminal A helix does not participate in the formation of the intermediate under our experimental conditions, because it is held at a distance from the C-terminal part of the protein by force. As a consequence, the intermediate seen here contains fewer stabilizing contacts and is thermodynamically weaker. Similarly, spatially biasing the A-helix away from the remainder of the protein may allow us to observe the intermediate in our experiments, in contrast to other geometries (*27*).

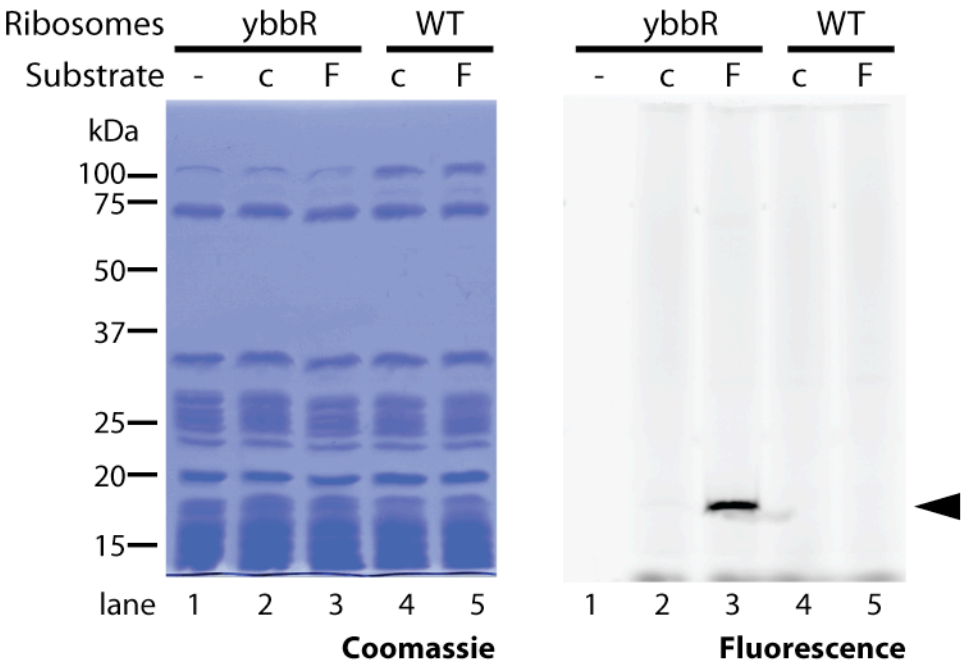

Fig. S1.

Specificity of L17 modification in tagged ribosomes. Isolated ybbR-tagged (lanes 1-3) or WT (lanes 4 and 5) ribosomes were incubated with Sfp enzyme in the presence of a fluorescent CoA adduct (F; lanes 3 and 5) or a control substrate (c; lanes 2 and 4) or in the absence of a substrate (lane 1). After separation of samples on SDS-PAGE gels, the fluorescence was imaged (right panel) and proteins were subsequently visualized by Coomassie staining. Coomassie staining revealed the typical ribosomal protein pattern. Fluorescence imaging revealed that a single protein band (arrowhead) is labeled in the ybbR-tagged ribosome sample, demonstrating the specificity of the Sfp-mediated reaction. No labeling is detected in the control reactions with either untagged ribosomes (lanes 4 and 5) or a control substrate (lane 2).

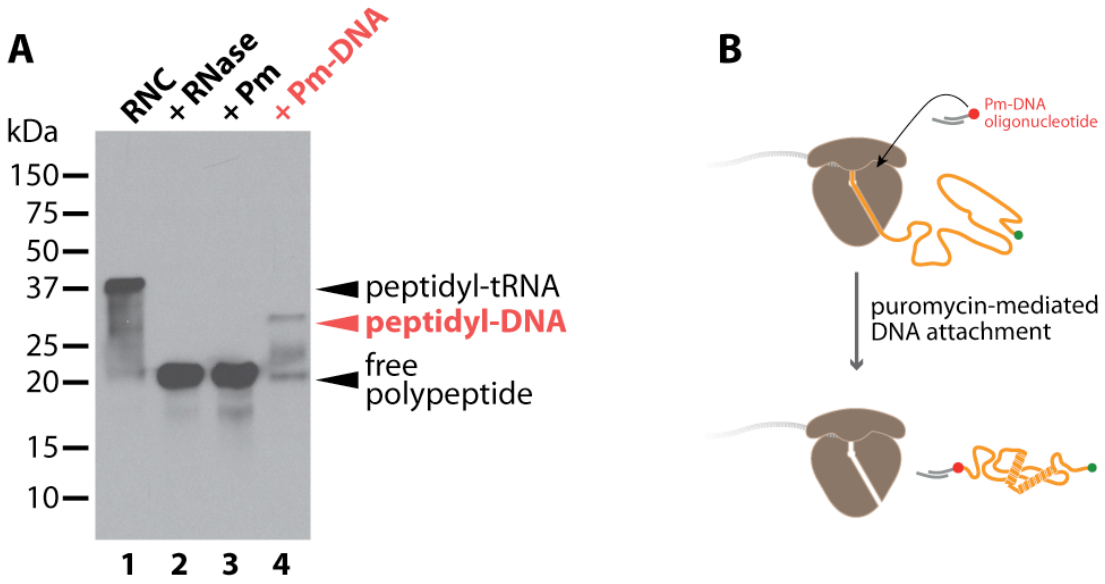

Fig. S2

(A) Western blot of stalled *in vitro* translation product. After translation of stop codon-free mRNA, RNCs were sedimented through 1M sucrose cushions. Samples were treated with RNase A ("RNase", 100 µg/ml), puromycin ("Pm", 1 mM) or puromycin-DNA oligonucleotides ("Pm-DNA", 10 µM) as indicated and separated on SDS-PAGE gels. Proteins were electro-blotted onto nitrocellulose membranes and detected with streptavidin-HRP by means of their biotin moiety. The electrophoretic mobility indicates that the translation product accumulates as a peptidyl-tRNA species (Lane 1; calculated Mw of the protein: 20.5 kDa; observed apparent Mw: ~38 kDa). RNase A treatment reverts the electrophoretic mobility to the expected value of ~20 kDa (Lane 2). Puromycin treatment also reverts the apparent Mw to 20 kDa (Lane 3). Since puromycin is incorporated into the nascent chain by the ribosome, this observation indicates that the peptidyl-tRNA is still anchored in the peptidyl transferase center. Incubation with a puromycin-derivatized DNA oligonucleotide results in the (partial) formation of a peptidyl-DNA species with an apparent Mw of ~30 kDa. **(B)** Schematic illustration of DNA handle attachment through puromycin-DNA oligonucleotides. The derivatized oligonucleotide is incubated with ribosome-bound nascent chains. Ribosome-mediated incorporation of the puromycin moiety results in covalent attachment of the oligonucleotide to the C-terminus and release of the nascent chain.

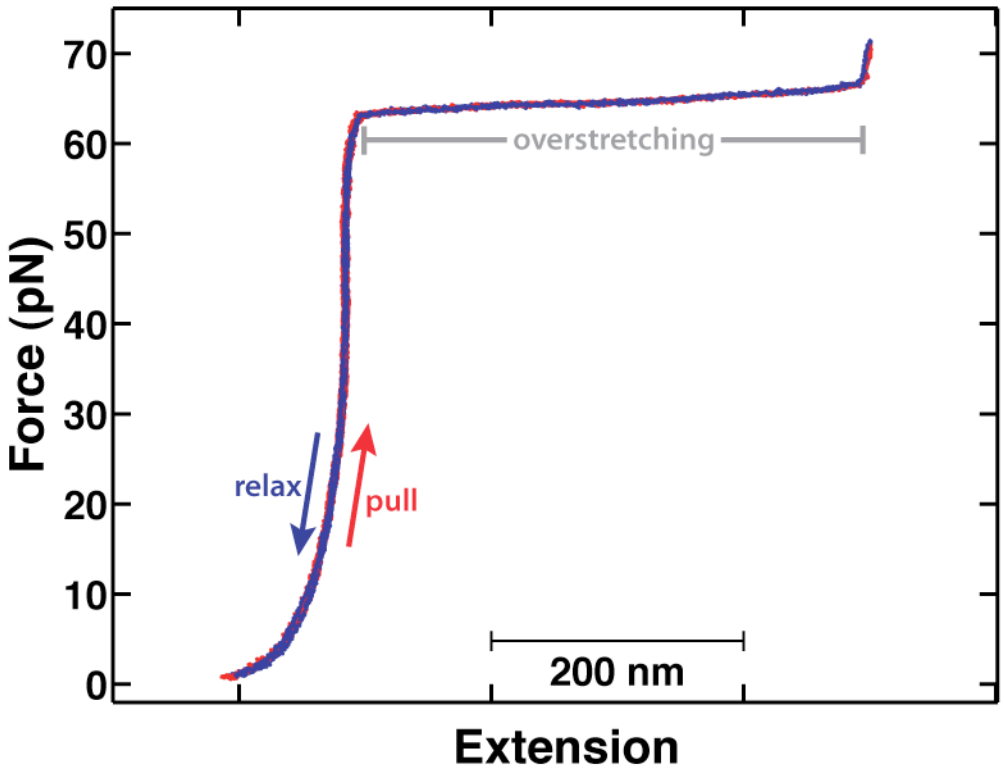

Fig. S3

Force-extension curves of DNA handles. A 1789 bp long fragment of DNA was synthesized directly on the surface of the bead in a bulk PCR-like reaction. A single molecule of this DNA was stretched (red curves) and relaxed (blue curves) repeatedly in the optical tweezers instrument. The curvature at forces below ~10 pN, due to the entropic elasticity of the molecule, and the overstretching plateau at ~65 pN are characteristic for double-stranded DNA. The molecule persists over several rounds of stretching to high forces (~70 pN), demonstrating stable attachment, and does not exhibit hysteresis upon relaxation, indicating that it is free of nicks.

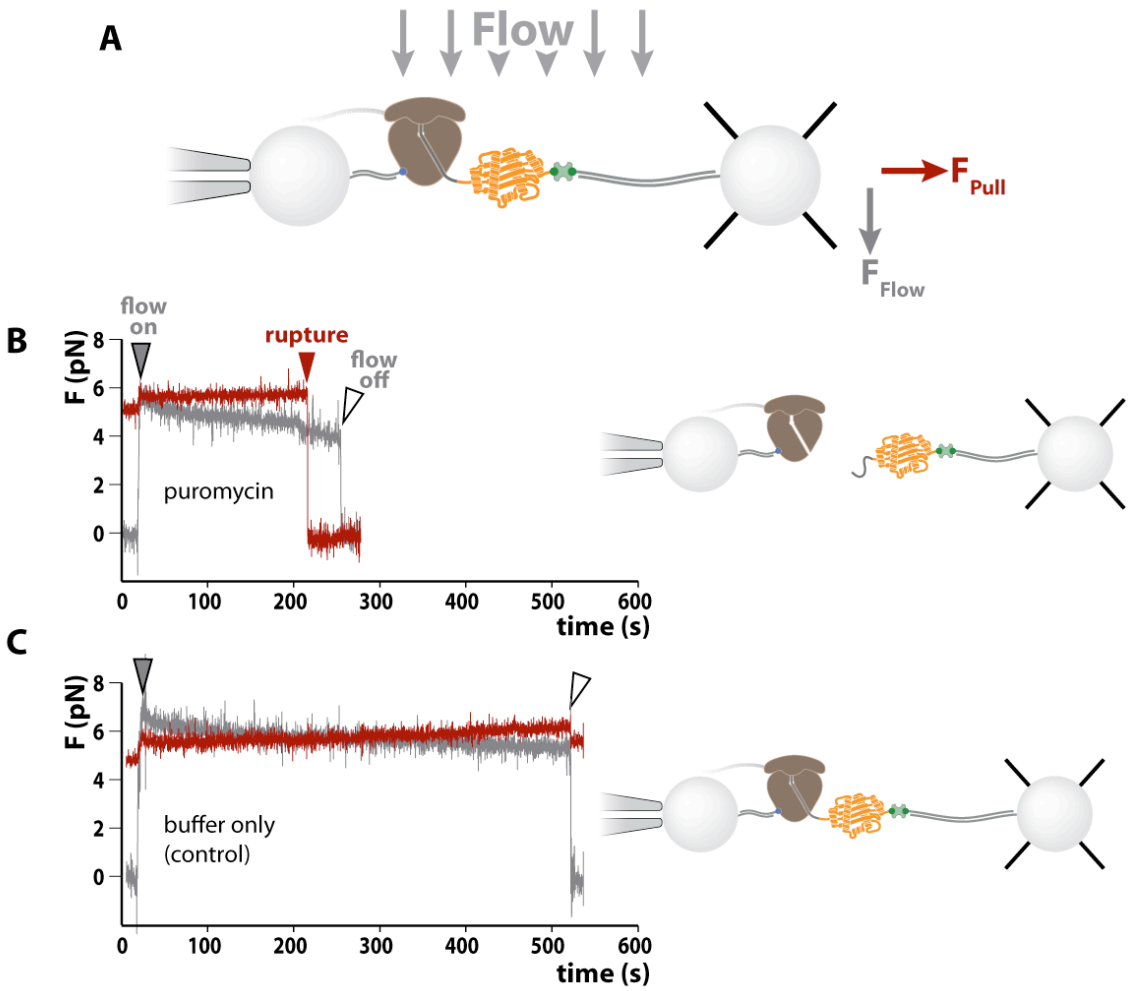

Fig. S4

Single-molecule puromycin release experiment. **(A)** Schematic of the experimental setup. A tether is formed with a RNC and held at a constant low force (F_{Pull} ≈ 5 pN). A solution of 1 mM puromycin is flowed into the chamber, resulting in a drag force on the bead (F_{Flow}) perpendicular to F_{Pull}. During the experiment, the forces F_{Pull} and F_{Flow} are recorded over time. **(B)** Puromycin release experiment (red trace: F_{Pull}, grey trace: F_{Flow}). A RNC tether is held at 5 pN constant force. At t ≈ 20 s, the flow of the puromycin into the microchamber is initiated (grey arrowhead). At t ≈ 220 s (when the puromycin that is being flowed into the chamber reaches the area around the trapped bead), the tether ruptures, indicated by a drop in F_{Pull} to 0 pN (red arrowhead). The flow of puromycin is stopped at t ≈ 260 s, and F_{Pull} also returns to 0 pN. (open grey arrowhead). **(C)** Buffer only control. Instead of puromycin, buffer is flowed into the chamber under conditions similar to those described in (A). The tether does not rupture over the course of the experiment (~500 s). Note that the tether is still intact when the recording stops at t ≈ 550 s.

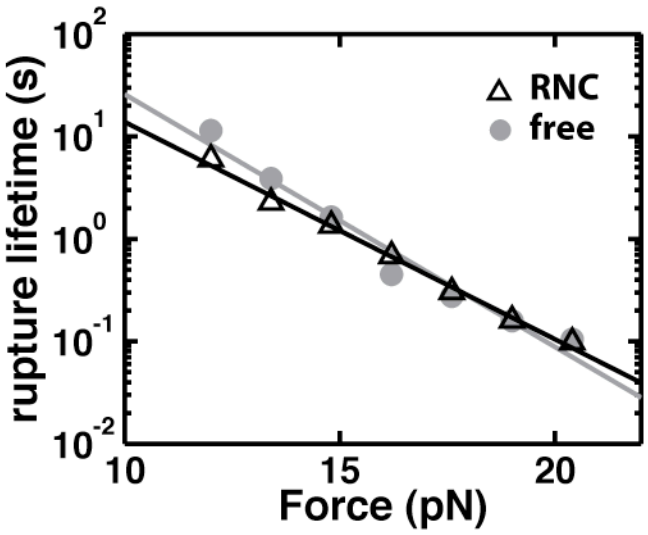

Fig. S5

Force-dependent lifetimes of free (circles) and ribosome-bound (triangles) T4 lysozyme. Very similar lifetimes were obtained from rupture-force distributions shown in Figure 1G and H according to Dudko *et al.* (ref (*35*)) for the ribosome-bound and free proteins, respectively. The lines represent fits based on Kramer's theory (see ref. (*35*)) with a scaling factor of $\nu = 1$, which reduces to Bell's formula. Varying the scaling factor over a range of $\nu = 1/2$ to $\nu = 1$ changed the values obtained from the fitting but did not affect the similitude of the values for free and ribosome-bound T4 lysozyme. The transitions state distances are very similar in both cases ($\Delta x_{free}^{\ddagger} = 2.3 \pm 0.5$ nm, $\Delta x_{ribosome\text{-}bound}^{\ddagger} = 2.0 \pm 0.2$ nm). The native state lifetimes at F = 0 pN of $\tau_{0,free} = 7503$ s (95% CI: 1053 s, 53637 s) and $\tau_{0,ribosome\text{-}bound} = 1826$ s (95% CI: 912 s, 3652 s) are afflicted with large errors because their determination is based on extrapolation, since the low force regime close to F = 0 pN is not accessible in these force ramp experiments.

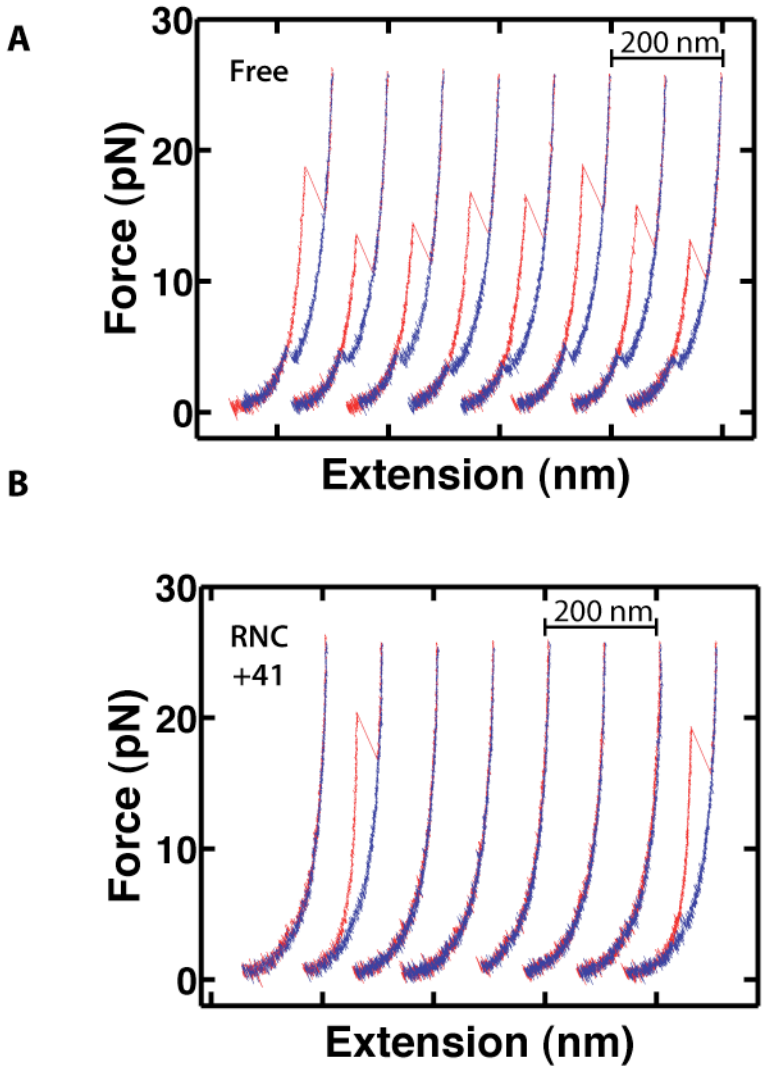

Fig. S6

Force-extension curves for free T4 lysozyme (A) and the "+41" RNC (B). Consecutive cycles of pulling (red) and relaxing (blue) the molecule are shown, offset along the x-axis for visual inspection. The traces recorded for the free protein exhibit unfolding transition at 14-19 pN during pulling, and a refolding transition is discernable at ~5 pN during relaxation. The refolding transition is not apparent in the RNC recordings, and unfolding is observed in only 2 of the 8 traces in this representative example.

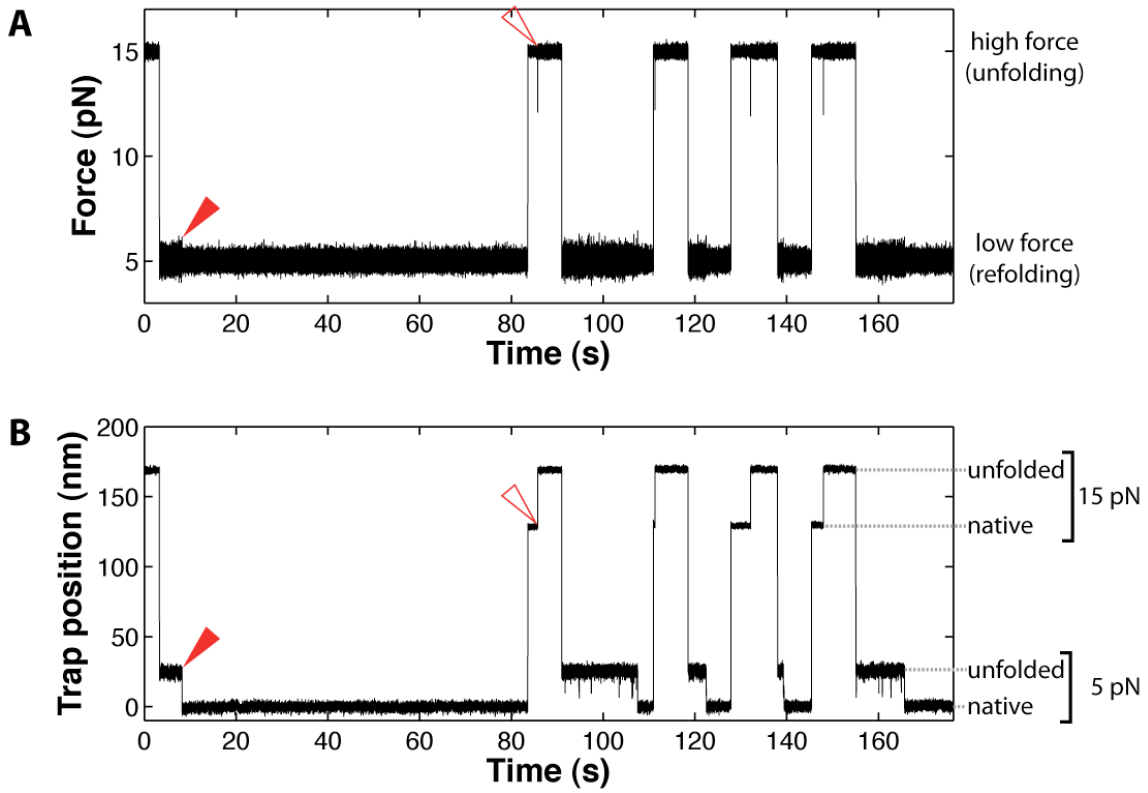

Fig. S7

Representative example of force clamp measurements of T4 lysozyme refolding (free protein). The force (A) and the position of the optical trap (B) are recorded over time, while the force is cycled between 5 pN and 15 pN. At 5 pN, the molecule refolds, indicated by a sudden compaction (red arrowhead). The molecule remains stably in the native state at this force, and no unfolding is observed over the course of 60 s. Raising the force to 15 pN destabilizes the folded protein and the molecule unfolds, indicated by a sudden increase in the extension (open arrowhead). The extension change upon unfolding at 15 pN (open arrowhead) is larger than the change upon refolding at 5 pN (solid arrowhead), in agreement with the entropic elasticity of the unfolded polypeptide which results in the unfolded state being more extended at 15 pN than at 5 pN.

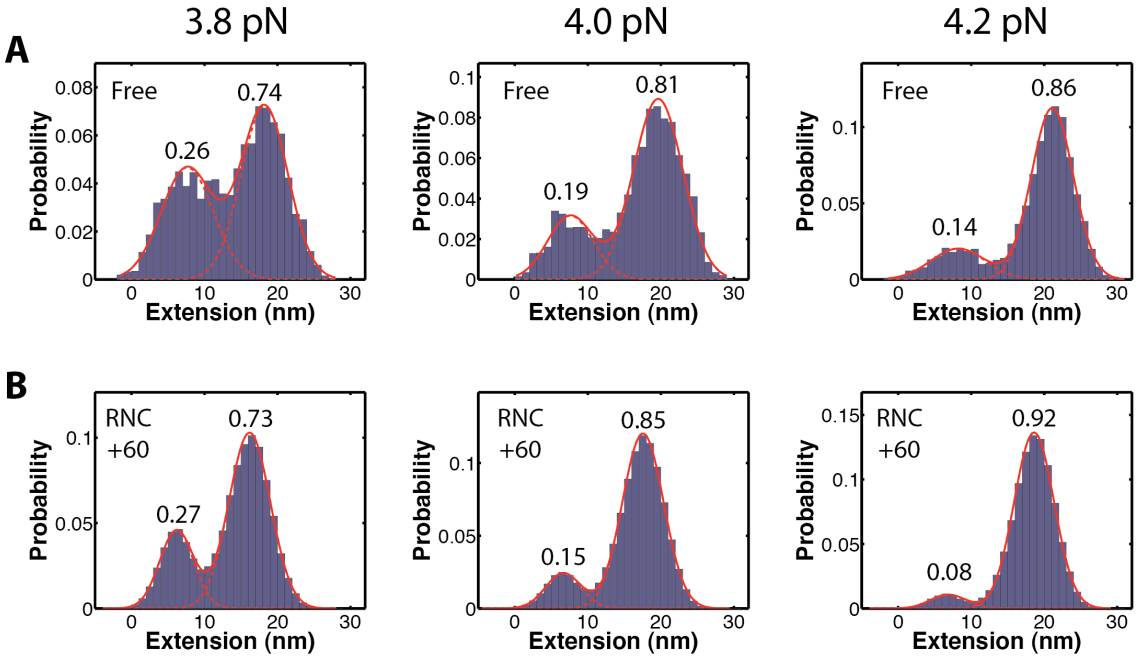

Fig. S8

Example histograms of state extensions of the unfolded and intermediate states. (A) Several refolding traces were recorded for a single free T4 lysozyme molecule during refolding at 3.8, 4.0 and 4.2 pN. The hopping between the unfolded and the intermediate state was analyzed. Extensions are relative to the native state (at 0 nm, not shown in the histograms). The extension data were fitted to a mixed Gaussian model with two components (solid red line). The individual components are plotted as dashed lines. The mixing proportions of the two components reflect the relative population of the unfolded and intermediate states prior to refolding. Increasing the force during refolding biases the molecule towards increasingly populating the unfolded state. (B) Same as in (A), recorded for a single "+60" RNC molecule. The numbers above the peaks represent the probabilities of the respective state as determined by fitting to the mixed Gaussian model. The shape of the histograms in (B) better approximates the mixed Gaussian model than the histograms in (A), because the reduced folding rates on the ribosome allow us to collect more data points. However, the relative probabilities for U and I at a given force are similar for the free and the ribosome-bound protein.

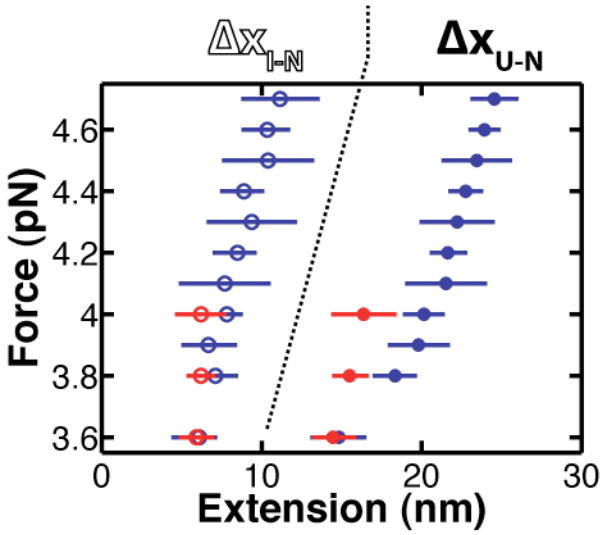

Fig. S9

Extension changes from BHMM analysis of force-clamp refolding experiments (open circles: $\Delta x_{I\text{-}N}$, filled circles: $\Delta x_{U\text{-}N}$) for the free (blue) and the ribosome-bound protein ("+60" construct, red).

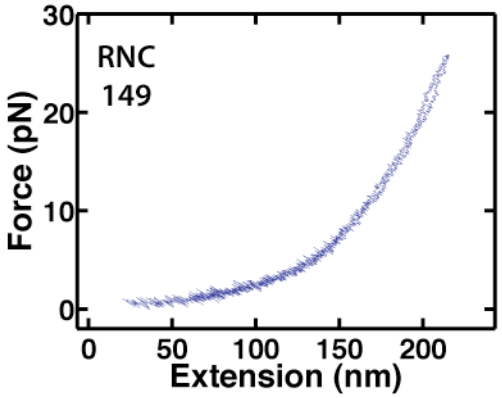

Fig. S10

Force extension curves recorded with ribosome-bound nascent chains comprising 149 N-terminal residues of T4 lysozyme (full-length T4 lysozyme: 164 amino acids). The traces do not exhibit any unfolding transitions, indicating that the nascent polypeptide does not acquire any stable structures.

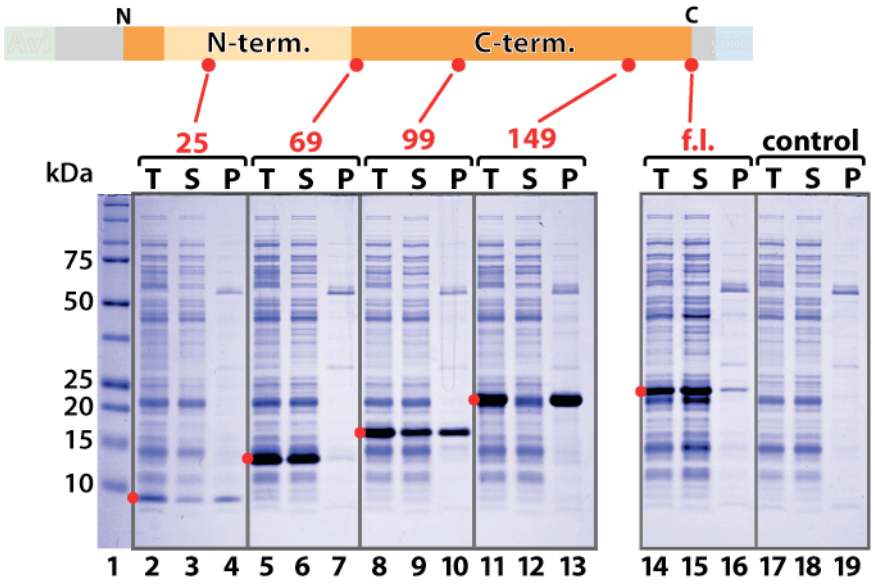

Fig. S11

Expression of T4 lysozyme fragments in *E. coli*. Fragments of T4 lysozyme composed of 25, 69, 99 and 149 N-terminal amino acids were expressed in *E. coli* BL21(DE3) cells from pET-based plasmids by induction with 1 mM IPTG for 2 h. All constructs contained an N-terminal Avi-tag and a C-terminal ybbR-tag. The lengths of the fragments are indicated by red dots in the diagram of the T4 lysozyme primary structure (top panel). Total cell extracts (T) were prepared by lysis under non-denaturing conditions and separated into soluble (S) and pellet (P) fractions by centrifugation at 20,000 *g*. T, S and P fractions were separated by SDS-PAGE. Proteins were stained with Coomassie Brilliant Blue. The positions of bands representing the overexpressed proteins are indicated by red dots (bottom panel). The 25 (lanes 2-4), 99 (lanes 8-10) and 149 (lanes 11-13) amino acid fragments are largely insoluble, indicating misfolding and aggregation of the translation products. The 69 amino acid fragment (lanes 5-7) comprising the N-terminal subdomain is largely soluble, similar to the full length protein ("f.l."; lanes 14-16) shown for reference. "control": uninduced sample (no overexpression; lanes 17-19)

References and Notes

1. C. B. Anfinsen, Principles that govern the folding of protein chains. *Science* **181**, 223 (1973). doi:10.1126/science.181.4096.223 Medline

2. J. Kubelka, T. K. Chiu, D. R. Davies, W. A. Eaton, J. Hofrichter, Sub-microsecond protein folding. *J. Mol. Biol.* **359**, 546 (2006). doi:10.1016/j.jmb.2006.03.034 Medline

3. K. W. Plaxco, K. T. Simons, D. Baker, Contact order, transition state placement and the refolding rates of single domain proteins. *J. Mol. Biol.* **277**, 985 (1998). doi:10.1006/jmbi.1998.1645 Medline

4. D. J. Brockwell, S. E. Radford, Intermediates: Ubiquitous species on folding energy landscapes? *Curr. Opin. Struct. Biol.* **17**, 30 (2007). doi:10.1016/j.sbi.2007.01.003 Medline

5. J. B. Udgaonkar, Multiple routes and structural heterogeneity in protein folding. *Annu. Rev. Biophys.* **37**, 489 (2008). doi:10.1146/annurev.biophys.37.032807.125920 Medline

6. J. P. Ellis, C. K. Bakke, R. N. Kirchdoerfer, L. M. Jungbauer, S. Cavagnero, Chain dynamics of nascent polypeptides emerging from the ribosome. *ACS Chem. Biol.* **3**, 555 (2008). doi:10.1021/cb800059u Medline

7. M. S. Evans, I. M. Sander, P. L. Clark, Cotranslational folding promotes β-helix formation and avoids aggregation in vivo. *J. Mol. Biol.* **383**, 683 (2008). doi:10.1016/j.jmb.2008.07.035 Medline

8. S. T. Hsu *et al*., Structure and dynamics of a ribosome-bound nascent chain by NMR spectroscopy. *Proc. Natl. Acad. Sci. U.S.A.* **104**, 16516 (2007). doi:10.1073/pnas.0704664104 Medline

9. A. Khushoo, Z. Yang, A. E. Johnson, W. R. Skach, Ligand-driven vectorial folding of ribosome-bound human CFTR NBD1. *Mol. Cell* **41**, 682 (2011). doi:10.1016/j.molcel.2011.02.027 Medline

10. J. Lu, C. Deutsch, Folding zones inside the ribosomal exit tunnel. *Nat. Struct. Mol. Biol.* **12**, 1123 (2005). doi:10.1038/nsmb1021 Medline

11. C. A. Woolhead, P. J. McCormick, A. E. Johnson, Nascent membrane and secretory proteins differ in FRET-detected folding far inside the ribosome and in their exposure to ribosomal proteins. *Cell* **116**, 725 (2004). doi:10.1016/S0092-8674(04)00169-2 Medline

12. S. Bhushan *et al*., α-helical nascent polypeptide chains visualized within distinct regions of the ribosomal exit tunnel. *Nat. Struct. Mol. Biol.* **17**, 313 (2010). doi:10.1038/nsmb.1756 Medline

13. R. Green, H. F. Noller, Ribosomes and translation. *Annu. Rev. Biochem.* **66**, 679 (1997). doi:10.1146/annurev.biochem.66.1.679 Medline

14. S. Varenne, J. Buc, R. Lloubes, C. Lazdunski, Translation is a non-uniform process. Effect of tRNA availability on the rate of elongation of nascent polypeptide chains. *J. Mol. Biol.* **180**, 549 (1984). doi:10.1016/0022-2836(84)90027-5 Medline

15. G. Cannarozzi *et al*., A role for codon order in translation dynamics. *Cell* **141**, 355 (2010). doi:10.1016/j.cell.2010.02.036 Medline

16. X. Qu *et al*., The ribosome uses two active mechanisms to unwind messenger RNA during translation. *Nature* **475**, 118 (2011). doi:10.1038/nature10126 Medline

17. C. Kimchi-Sarfaty *et al*., A "silent" polymorphism in the *MDR*1 gene changes substrate specificity. *Science* **315**, 525 (2007). doi:10.1126/science.1135308 Medline

18. G. Zhang, M. Hubalewska, Z. Ignatova, Transient ribosomal attenuation coordinates protein synthesis and co-translational folding. *Nat. Struct. Mol. Biol.* **16**, 274 (2009). doi:10.1038/nsmb.1554 Medline

19. E. Siller, D. C. DeZwaan, J. F. Anderson, B. C. Freeman, J. M. Barral, Slowing bacterial translation speed enhances eukaryotic protein folding efficiency. *J. Mol. Biol.* **396**, 1310 (2010). doi:10.1016/j.jmb.2009.12.042 Medline

20. S. T. Liang, Y. C. Xu, P. Dennis, H. Bremer, mRNA composition and control of bacterial gene expression. *J. Bacteriol.* **182**, 3037 (2000). doi:10.1128/JB.182.11.3037-3044.2000 Medline

21. C. C. Chow *et al*., Chain length dependence of apomyoglobin folding: Structural evolution from misfolded sheets to native helices. *Biochemistry* **42**, 7090 (2003). doi:10.1021/bi0273056 Medline

22. A. H. Elcock, Molecular simulations of cotranslational protein folding: Fragment stabilities, folding cooperativity, and trapping in the ribosome. *PLoS Comput. Biol.* **2**, e98 (2006). doi:10.1371/journal.pcbi.0020098 Medline

23. E. P. O'Brien, S. T. Hsu, J. Christodoulou, M. Vendruscolo, C. M. Dobson, Transient tertiary structure formation within the ribosome exit port. *J. Am. Chem. Soc.* **132**, 16928 (2010). doi:10.1021/ja106530y Medline

24. J. R. Moffitt, Y. R. Chemla, S. B. Smith, C. Bustamante, Recent advances in optical tweezers. *Annu. Rev. Biochem.* **77**, 205 (2008). doi:10.1146/annurev.biochem.77.043007.090225 Medline

25. A. Ashkin, J. M. Dziedzic, J. E. Bjorkholm, S. Chu, Observation of a single-beam gradient force optical trap for dielectric particles. *Opt. Lett.* **11**, 288 (1986). doi:10.1364/OL.11.000288 Medline

26. H. Dietz, M. Rief, Protein structure by mechanical triangulation. *Proc. Natl. Acad. Sci. U.S.A.* **103**, 1244 (2006). doi:10.1073/pnas.0509217103 Medline

27. E. A. Shank, C. Cecconi, J. W. Dill, S. Marqusee, C. Bustamante, The folding cooperativity of a protein is controlled by its chain topology. *Nature* **465**, 637 (2010). doi:10.1038/nature09021 Medline

28. M. Matsumura, B. W. Matthews, Control of enzyme activity by an engineered disulfide bond. *Science* **243**, 792 (1989). doi:10.1126/science.2916125 Medline

29. J. Cellitti *et al*., Exploring subdomain cooperativity in T4 lysozyme I: Structural and energetic studies of a circular permutant and protein fragment. *Protein Sci.* **16**, 842 (2007). doi:10.1110/ps.062628607 Medline

30. M. Llinás, S. Marqusee, Subdomain interactions as a determinant in the folding and stability of T4 lysozyme. *Protein Sci.* **7**, 96 (1998). doi:10.1002/pro.5560070110 Medline

31. W. A. Baase, L. Liu, D. E. Tronrud, B. W. Matthews, Lessons from the lysozyme of phage T4. *Protein Sci.* **19**, 631 (2010). doi:10.1002/pro.344 Medline

32. Materials and methods and additional information are available as supporting material on *Science* Online.

33. N. R. Voss, M. Gerstein, T. A. Steitz, P. B. Moore, The geometry of the ribosomal polypeptide exit tunnel. *J. Mol. Biol.* **360**, 893 (2006). doi:10.1016/j.jmb.2006.05.023 Medline

34. C. Bustamante, J. F. Marko, E. D. Siggia, S. Smith, Entropic elasticity of λ-phage DNA. *Science* **265**, 1599 (1994). doi:10.1126/science.8079175 Medline

35. O. K. Dudko, G. Hummer, A. Szabo, Theory, analysis, and interpretation of single-molecule force spectroscopy experiments. *Proc. Natl. Acad. Sci. U.S.A.* **105**, 15755 (2008). doi:10.1073/pnas.0806085105 Medline

36. P. Weinkam, E. V. Pletneva, H. B. Gray, J. R. Winkler, P. G. Wolynes, Electrostatic effects on funneled landscapes and structural diversity in denatured protein ensembles. *Proc. Natl. Acad. Sci. U.S.A.* **106**, 1796 (2009). doi:10.1073/pnas.0813120106 Medline

37. J. Cellitti, R. Bernstein, S. Marqusee, Exploring subdomain cooperativity in T4 lysozyme II: Uncovering the C-terminal subdomain as a hidden intermediate in the kinetic folding pathway. *Protein Sci.* **16**, 852 (2007). doi:10.1110/ps.062632807 Medline

38. C. Bustamante, Y. R. Chemla, N. R. Forde, D. Izhaky, Mechanical processes in biochemistry. *Annu. Rev. Biochem.* **73**, 705 (2004). doi:10.1146/annurev.biochem.72.121801.161542 Medline

39. R. Liu, J. E. Barrick, J. W. Szostak, R. W. Roberts, Optimized synthesis of RNA-protein fusions for in vitro protein selection. *Methods Enzymol.* **318**, 268 (2000). doi:10.1016/S0076-6879(00)18058-9 Medline

40. C. Voisset, S. J. Saupe, M. Blondel, The various facets of the protein-folding activity of the ribosome. *Biotechnol. J.* **6**, 668 (2011). doi:10.1002/biot.201100021 Medline

41. G. de Prat Gay *et al*., Conformational pathway of the polypeptide chain of chymotrypsin inhibitor-2 growing from its N terminus in vitro. Parallels with the protein folding pathway. *J. Mol. Biol.* **254**, 968 (1995). doi:10.1006/jmbi.1995.0669 Medline

42. J. L. Neira, A. R. Fersht, Exploring the folding funnel of a polypeptide chain by biophysical studies on protein fragments. *J. Mol. Biol.* **285**, 1309 (1999). doi:10.1006/jmbi.1998.2249 Medline

43. H. Taniuchi, Formation of randomly paired disulfide bonds in des-(121-124)-ribonuclease after reduction and reoxidation. *J. Biol. Chem.* **245**, 5459 (1970). Medline

44. F. U. Hartl, M. Hayer-Hartl, Molecular chaperones in the cytosol: From nascent chain to folded protein. *Science* **295**, 1852 (2002). doi:10.1126/science.1068408 Medline

45. B. Schuler, E. A. Lipman, W. A. Eaton, Probing the free-energy surface for protein folding with single-molecule fluorescence spectroscopy. *Nature* **419**, 743 (2002). doi:10.1038/nature01060 Medline

46. F. Brandt *et al*., The native 3D organization of bacterial polysomes. *Cell* **136**, 261 (2009). doi:10.1016/j.cell.2008.11.016 Medline

47. H. X. Zhou, K. A. Dill, Stabilization of proteins in confined spaces. *Biochemistry* **40**, 11289 (2001). doi:10.1021/bi0155504 Medline

48. J. Mittal, R. B. Best, Thermodynamics and kinetics of protein folding under confinement. *Proc. Natl. Acad. Sci. U.S.A.* **105**, 20233 (2008). doi:10.1073/pnas.0807742105 Medline

49. J. Kiraga *et al*., The relationships between the isoelectric point and length of proteins, taxonomy and ecology of organisms. *BMC Genomics* **8**, 163 (2007). doi:10.1186/1471-2164-8-163 Medline

50. J. Yin *et al*., Genetically encoded short peptide tag for versatile protein labeling by Sfp phosphopantetheinyl transferase. *Proc. Natl. Acad. Sci. U.S.A.* **102**, 15815 (2005). doi:10.1073/pnas.0507705102 Medline

51. K. A. Datsenko, B. L. Wanner, One-step inactivation of chromosomal genes in *Escherichia coli* K-12 using PCR products. *Proc. Natl. Acad. Sci. U.S.A.* **97**, 6640 (2000). doi:10.1073/pnas.120163297 Medline

52. G. Spedding, in *Ribosomes and Protein Synthesis: A Practical Approach*, G. Spedding, Ed. (Oxford Univ. Press, Oxford, 1990), pp. 1–29.

53. J. Yin, A. J. Lin, D. E. Golan, C. T. Walsh, Site-specific protein labeling by Sfp phosphopantetheinyl transferase. *Nat. Protoc.* **1**, 280 (2006). doi:10.1038/nprot.2006.43 Medline

54. D. Beckett, E. Kovaleva, P. J. Schatz, A minimal peptide substrate in biotin holoenzyme synthetase-catalyzed biotinylation. *Protein Sci.* **8**, 921 (1999). doi:10.1110/ps.8.4.921 Medline

55. S. B. Smith, Y. Cui, C. Bustamante, Overstretching B-DNA: The elastic response of individual double-stranded and single-stranded DNA molecules. *Science* **271**, 795 (1996). doi:10.1126/science.271.5250.795 Medline

56. Y. Shimizu *et al*., Cell-free translation reconstituted with purified components. *Nat. Biotechnol.* **19**, 751 (2001). doi:10.1038/90802 Medline

57. D. N. Fuller *et al*., A general method for manipulating DNA sequences from any organism with optical tweezers. *Nucleic Acids Res.* **34**, e15 (2006). doi:10.1093/nar/gnj016 Medline

58. S. B. Smith, Y. Cui, C. Bustamante, Optical-trap force transducer that operates by direct measurement of light momentum. *Methods Enzymol.* **361**, 134 (2003). doi:10.1016/S0076-6879(03)61009-8 Medline

59. C. Cecconi, E. A. Shank, C. Bustamante, S. Marqusee, Direct observation of the three-state folding of a single protein molecule. *Science* **309**, 2057 (2005). doi:10.1126/science.1116702 Medline

60. C. P. Robert, G. Celeux, J. Diebolt, Bayesian estimation of hidden Markov chains: A stochastic implementation. *Stat. Probab. Lett.* **16**, 77 (1993). doi:10.1016/0167-7152(93)90127-5

61. S. A. McKinney, C. Joo, T. Ha, Analysis of single-molecule FRET trajectories using hidden Markov modeling. *Biophys. J.* **91**, 1941 (2006). doi:10.1529/biophysj.106.082487 Medline

62. F. Noé, Probability distributions of molecular observables computed from Markov models. *J. Chem. Phys.* **128**, 244103 (2008). doi:10.1063/1.2916718 Medline

63. H. Kato, H. Feng, Y. Bai, The folding pathway of T4 lysozyme: The high-resolution structure and folding of a hidden intermediate. *J. Mol. Biol.* **365**, 870 (2007). doi:10.1016/j.jmb.2006.10.047 Medline